

Numerical investigations on rotor dynamic stall of horizontal axis wind turbine

I. Yous et R. Dizene

Laboratoire de Mécanique Avancée, Université des Sciences et de la Technologie Houari Boumediene, B.P. 32, El Alia, Bab Ezzouar, Alger, Algérie

Abstract - Wind energy is rapidly becoming an economically viable energy source. This is partially due to increases in the cost of oil, but also due to significant improvements in the performance of modern wind turbines. Next generation of horizontal axis wind turbines (HAWT), including very tall wind turbine structure, will operate at high wind speeds (in excess of 15m/s). At these speeds, flow over the rotor is likely to be separated, at least partially over the rotor disk. The flow environment, and in particular the magnitude and frequency content of unsteady loads, should be well understood for structural design. Existing engineering approaches using a combination of 2-D airfoil tools and combined blade element and momentum theory are not adequate for modeling wind turbines at these high wind speeds. Because of the costs associated with performing wind tunnel experiments, there is a significant amount of interest in predicting the aerodynamic characteristics of a wind turbine using computational fluid dynamics (CFD).

Résumé - La présente publication porte sur l'étude des vents dans une région semi-aride afin de déterminer leur contribution dans l'avancée des sables vers le nord. Pour cela deux méthodes ont été utilisées. La première passe par le traitement des mesures relevées au niveau des stations météorologiques et la seconde par l'établissement de la carte des vitesses du vent de la région par l'extrapolation des mesures à 700 Hpa. Les deux méthodes ont montré que les vents dominants sont Nord et Ouest. Ceci montre que l'activité éolienne, dans les hauts plateaux, n'est pas la cause principale de l'avancée du sable. Par ailleurs, les vitesses moyennes annuelles et journalière varient en moyenne entre 4 et 5 m/s ce qui implique que les ressources énergétiques éoliennes de la région ne peuvent répondre qu'aux petites applications.

Mots clés: Erosion éolienne - Zone semi-aride - Modèle Aiolos - Vitesse moyenne - Vent dominant.

1. INTRODUCTION

The wind turbine industry is currently facing many difficulties constructing efficient wind turbine machines caused by the inability predict structural loading and power output. Available evidence from wind turbines in a field environment suggests that formation of complex unsteady separated flow fields may be responsible for many aspects of wind turbine component failure. Power output and structural loads have been inadequately predicted, leading to the failure of power generators, gearboxes, and even turbine blades. Because the corresponding loading and power output is caused by aerodynamic forces, the underlying fluid dynamics must be well understood to accurately determine structural and power requirements. To examine this possibility, unsteady state, 3-D simulation and wind-tunnel data are generally used to estimate aerodynamic loads on wind turbine blades.

A computational research program is underway at USTHB University in the area of horizontal-axis wind turbine aerodynamics. The research focuses on understanding the flow mechanisms that affect the performance of wind turbines operating in non-axial

and non-uniform inflow, and the development of modern, efficient computational techniques that complement existing combined blade element-momentum theory.

Some computational effort was based on the use of 3-D hybrid Navier-Stokes/potential flow calculation theories [1] that have been developed for helicopter rotor and propeller applications to horizontal axis wind turbines. In this approach three-dimensional unsteady compressible Navier-Stokes equations are solved in a small region, on a body-fitted grid surrounding the rotor blade. Away from the blades, the potential flow equation is solved. The vortices shed by the blades as a result of dynamic stall, and spanwise and azimuthal variations of the circulation are captured by vortex filaments that are freely convected by the local flow.

Wind energy represents one of the cleanest sources of energy available to mankind. Recent advances in airfoil and rotor development, materials technology, power generation systems and manufacturing technology have made wind turbine systems in general, and horizontal axis wind turbine (HAWT) systems in particular, economically feasible alternatives to gas, oil, and coal based power generation systems. References [2-4] and related publications discuss the technological and economic aspects of wind energy. Many of the rotors found on current generation HAWT systems are designed using a combination of 2-D airfoil tools [4-7] and three-dimensional blade element and momentum (BEM) theory [8].

A number of comprehensive computer codes using this methodology are currently available to the designer. In these methods, unsteady flow effects are either ignored, or modeled using a synthesis of 2-D data [9]. As a result, these methods are incapable of accurately modelling three-dimensional dynamic stall processes, tower shadow effects, tip relief effects, and sweep effects.

These three-dimensional effects can alter the air loads, affect the fatigue life, and significantly influence the cost of ownership of HAWT systems. Although first-principles based modelling of the aerodynamics of HAWT systems is a viable approach, the cost of such detailed simulations based on Navier-Stokes equations limit their use to explorative studies.

2. GEOMETRY AND COMPUTATIONAL MESH

The first objective of this work is to perform a comprehensive turbulence model evaluation. This can be achieved by following closely the guidelines of the model selection process. The unsteady aerodynamics of turbulence modeling is based on the two-wide used methods: Reynolds Averaged Navier-Stokes equations (RANS) and Large Eddy Simulation (LES).

This study uses the ANSYS-CFX, a commercial CFD code, to make a 3-D flow analysis and performance evaluation of the linear taper and non-linear twist blade with an S809 airfoil of the NREL/NASA Ames Phase-VI rotor at zero degree yaw angle. A moving frame approach is used to solve the equations in steady-state mode based on the two-equation $k-\omega$ and SST turbulence model and the forces (i.e. lift and drag) are monitored in order to judge convergence.

A relatively large time step of 1/5 the airfoil characteristic time (i.e. chord/relative free-stream velocity/5) was specified and this was possible due to the implicit nature of the CFX code. The CFD grid for this case consisted of an O-type mesh of approximately 1 million nodes with a maximum y^+ of one and was created using the ICEM grid generator. The model used to compute the NREL wind turbine is illustrated in Figure 1.

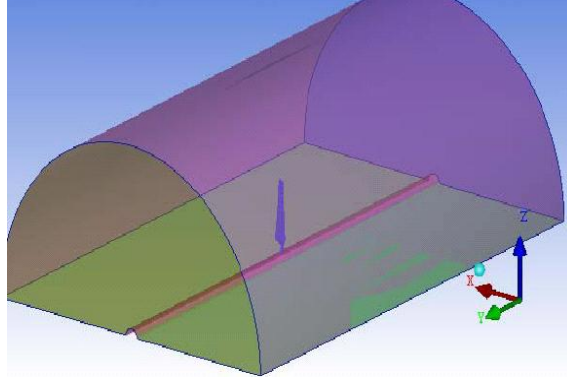


Fig. 1: Calculation domain geometry in the wind tunnel configuration and the blade topology

The mathematical formulation behind the Navier-Stokes is described and numerical results are presented for a rotor tested at the National Renewable Energy Laboratory under the Combined Experiment Rotor (CER) program which is referred to as the Phase VI rotor in NREL documentation. The second blade was modelled using a periodic boundary condition at the hub and farfield boundary conditions were located at approximately twice the rotor diameter. The inlet turbulence intensity specified for the CFD computations was 1%. Fully turbulent CFD runs were made for a wind speeds between 7 m/s and 25 m/s.

3. NUMERICAL METHOD

3.1 Basic equations

The relevant equations of motion for aerodynamic flows are the mass, momentum and energy equations:

$$\frac{\partial \bar{p}}{\partial t} + \frac{\partial (\bar{\rho} \tilde{u}_i)}{\partial x_i} = 0$$

$$\frac{\partial (\bar{\rho} \tilde{u}_i)}{\partial t} + \frac{\partial (\bar{\rho} \tilde{u}_i \tilde{u}_j)}{\partial x_j} = -\frac{\partial \bar{p}}{\partial x_i} + \frac{\partial}{\partial x_j} \left[\bar{\tau}_{ij} - \overline{\rho u'_i u'_j} \right]$$

Where $\bar{\tau}_{ij} = \mu \left[\left(\frac{\partial \bar{u}_i}{\partial x_j} + \frac{\partial \bar{u}_j}{\partial x_i} \right) - \frac{2}{3} \delta_{ij} \frac{\partial \bar{u}_k}{\partial x_k} \right]$ is the stress tensor.

$$\begin{aligned} \frac{\partial (\bar{\rho} \tilde{h})}{\partial t} + \frac{\partial (\bar{\rho} \tilde{h} \tilde{u}_j)}{\partial x_j} &= \frac{\partial \bar{p}}{\partial t} + \tilde{u}_j \frac{\partial \bar{p}}{\partial x_j} + \overline{u'_j \frac{\partial p}{\partial x_j}} + \\ &\frac{\partial}{\partial x_j} \left(-K \frac{\partial \bar{T}}{\partial x_j} - \overline{\rho h' \tilde{u}_j} \right) + \overline{\tau_{ij} \frac{\partial u'_i}{\partial x_j}} \end{aligned}$$

where h is the static enthalpy, u is the velocity, ρ is the density, p is the pressure and μ is the fluid viscosity.

3.2 Turbulence modeling

Menter [10] combines the $k - \varepsilon$ and $k - \omega$ models in a way that would allow them to be used in the regions where they show to best advantage. In other words, the method uses the $k - \omega$ model near the wall, but switches through a function F_1 to the $k - \varepsilon$ equations away from the wall, these equations having been transformed to a $k - \omega$ format. This method subsequently incorporates Bradshaw's suggestion that the Reynolds shear stress should be taken as being proportional to the turbulent kinetic energy. He calls this model as shear stress transport. The final equations are:

$$\frac{\partial(\rho k)}{\partial t} + \bar{u}_j \frac{\partial(\rho k)}{\partial x_j} = \tau_{ij} \frac{\partial \bar{u}}{\partial x_j} - \beta^* \rho \omega k + \frac{\partial}{\partial x_j} \left[(\mu + \sigma_k \mu_1) \frac{\partial k}{\partial x_j} \right]$$

$$\frac{\partial(\rho \omega)}{\partial t} + \bar{u}_j \frac{\partial(\rho \omega)}{\partial x_j} = \frac{\mu}{\mu_t} \tau_{ij} \frac{\partial \bar{u}}{\partial x_j} - \beta \rho \omega^2 + \frac{\partial}{\partial x_j} \left[(\mu + \sigma_\omega \mu_1) \frac{\partial \omega}{\partial x_j} \right]$$

$$+ 2(1 - F_1) \rho \sigma_\omega^2 \frac{1}{\omega} \frac{\partial k}{\partial x_i} \frac{\partial \omega}{\partial x_j}$$

The constants in the SST model are calculated as follows. If ϕ is the constant in the SST model and ϕ_1 and ϕ_2 are the constants in the $k - \omega$ model and the transformed $k - \varepsilon$ model, respectively, then

$$\phi = F_1 \cdot \phi_1 + (1 - F_1) \cdot \phi_2$$

The constants in the $k - \omega$ are:

$$\sigma_{k_1} = 0.85; \sigma_{\omega_1} = 0.5; \beta_1 = 0.075; a_1 = 0.31; \beta^* = 0.09;$$

$$K = 0.41; \gamma_1 = \frac{\beta_1}{\beta^*} - \frac{\sigma_{\omega_1} K^2}{\sqrt{\beta^*}}$$

The constants in the $k - \varepsilon$ are:

$$\sigma_{k_2} = 1.0; \sigma_{\omega_2} = 0.856; \beta_2 = 0.0828; \beta^* = 0.09; \beta_{k_1} = 0.075;$$

$$\gamma_1 = \frac{\beta_2}{\beta^*} - \frac{\sigma_{\omega_2} K^2}{\sqrt{\beta^*}}$$

$$\tau_{ij} \text{ is given by equation: } -\rho \overline{u_i' u_j'} = -\frac{2}{3} \rho k \delta_{ij} + \mu_i \left(\frac{\partial \bar{u}_i}{\partial x_j} + \frac{\partial \bar{u}_j}{\partial x_i} \right)$$

$$F_1 = \tanh \left(\arg_1^4 \right)$$

The grid generation is one of the most important stage of the numerical simulation and on which obtaining will depend on robust and reliable predictions. Before generating the grid in volume defining the field of calculation, the property of 180° periodicity rotor is taken into account, to reduce the field of calculation and not to generate as well as a grid around one only blade. The remaining blade is taken into

account in our calculations by using periodic boundary conditions. Our field of calculation is a half rolls 12.192 m of ray (height of the tower of the wind mill) and of 36.6 m length thus corresponding to the dimensions of the test wind tunnel section of the blower of NASA Hearts.

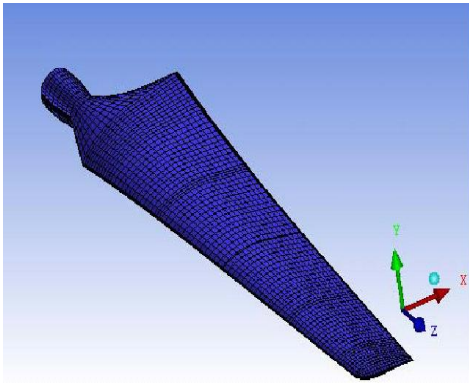


Fig. 2: The surface mesh used in our Study for the rotor blade

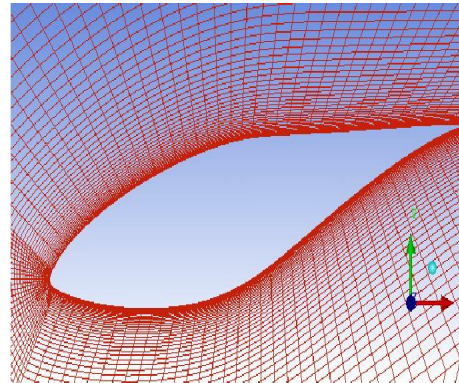


Fig. 3: Exponential distribution meshing near the S809 airfoil wall

5. RESULTS AND DISCUSSION

This section presents the first numerical results for the S809 NREL PHASE-VI rotor blade. Several 3-D wind turbine applications have been successfully treated within the NREL Phase-VI rotor configurations. The operational conditions are given in **Table 1**. Our objective is to perform a comprehensive turbulence model evaluation.

The turbulence model is important for the prediction of the point of the turbulent separation which determines the maximum of lift coefficient $C_{L\max}$. In the present version CFX uses either standard $k - \varepsilon$ by Launder, $k - \omega$ by Wilcox or the SST model by Menter.

Results of quantitative blade pressure distributions and velocity streamlines are presented for 10 m/s; 15 m/s and 20 m/s. Figure 4 shows the pressure coefficient (C_p) distribution and in every case we can see a form of classical distribution around the blade airfoil surfaces. The pressure on the suction side changes from a highly peaked form to a minimum value at the leading edge. For the case of 15 m/s velocity, the peak is located at 20 % span with a corresponding drop located at 10 % span on the pressure side. The pressure distributions observed at 10 m/s and at 20 m/s are significantly different: the upper surface pressure undergoes a fairly smooth drop from the trailing edge to the leading edge. The highly velocity peak observed at 15 m/s exhibit the expected features of stall which may be characterized by losses and vortex formation.

Figure 5 presents a spanwise streamlines velocity for the same velocity values. Some differences are observed from the tip blade edge to the root blade edge. Identification of a separation location other than leading edge or near trailing edge is not at all obvious. The lowest velocities are observed on the entire blade upper surface at 20 m/s; but at 15 m/s the results show some highest velocity region from the blade tip edge on half part of the upper surface and propagate towards the blade leading edge.

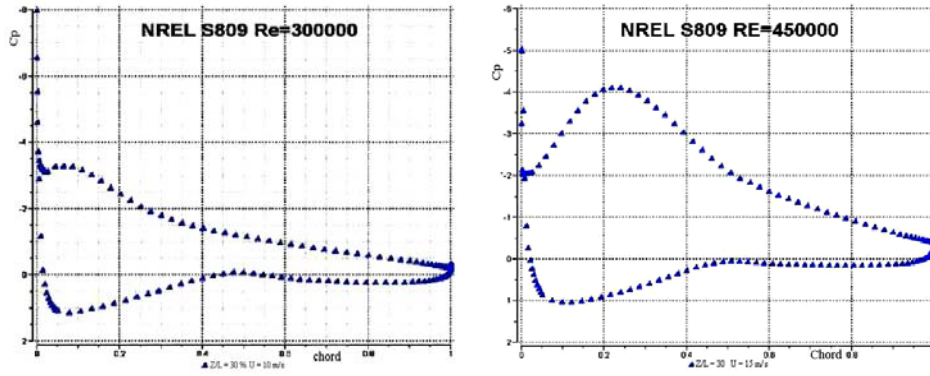


Fig. 4: Computed pressure coefficient distribution

Table 1: Test conditions of phase VI wind turbine (wind tunnel NASA Ames)

File name	Bracade blade angle (°)	Blade tip chock angle (°)	Wind tunnel temperature (°C)
S07000000	0	3	11.1
S10000000	0	3	11.0
S13000000	0	3	13.7
S15000000	0	3	14.2
S20000000	0	3	14.5
S25000000	0	3	14.4
S10000100	0	3	10.9
S13000100	0	3	13.7
S15000100	0	3	14.2
S10000300	0	3	10.9
S13000300	0	3	13.7
S15000300	0	3	14.0
S10000600	0	3	10.9
S15000600	0	3	13.9

Table 1: Test conditions of phase VI wind turbine (wind tunnel NASA Ames)_continue

Yaw angle (°)	Rotation speed (rpm)	Wind velocity (m/s)	Air density (kg/m ³)
0.0	71.9	7.0	1.246
0.0	72.1	10.0	1.246
0.0	72.1	13.1	1.227
0.0	72.1	15.1	1.224
0.1	72.0	20.1	1.221
-0.1	72.1	25.1	1.220
10.0	72.1	10.1	1.246
10.1	72.1	13.1	1.227
10.0	72.1	15.1	1.224
30.2	72.0	10.1	1.246
30.0	72.2	13.0	1.227
29.9	72.2	15.1	1.225
60.0	71.7	10.1	1.246
60.0	71.9	15.1	1.225

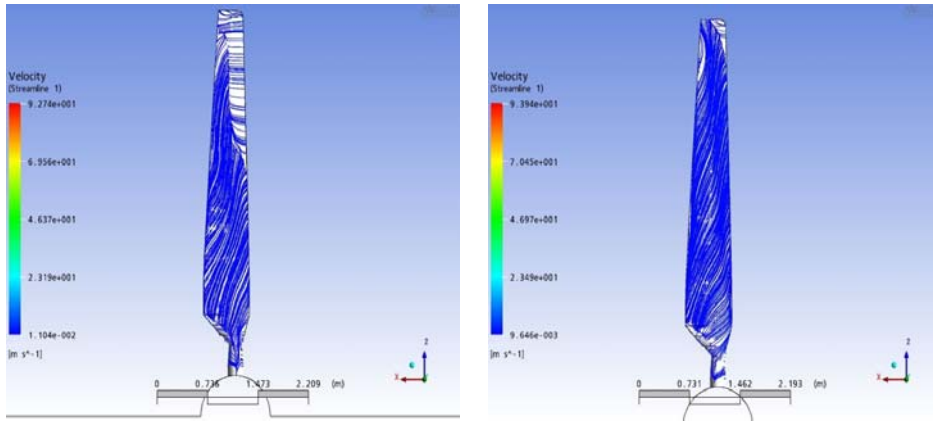


Fig. 5: Computed streamlines velocity

Acknowledgements - The authors wish to thank the NREL Laboratory for providing the NREL Phase-VI rotor configurations data.

NOMENCLATURE

T	Absolute temperature (K)	p	Pressure (Nm ⁻²)
K	Thermal conductivity	h	Specific enthalpy (Jkg ⁻¹)
k	Turbulent kinetic energy (m ² s ⁻²)	x	Direction axis (m)
u	Velocity (ms ⁻¹)		
	<i>Greek letters</i>	ε	Rate of dissipation of turbulent Kinetic energy (m ² s ⁻³)
μ	Dynamic viscosity (Wm ⁻²)	t	Time (s)
ρ	Density (kgm ⁻³)		<i>Superscripts</i>
	<i>Subscripts</i>	ˆ	Fluctuations quantities with
i, j, k	Quantities in x, y, z dimensions	˙	Respect to time
max	Maximum	≈	Mass-averaged quantities
turb max	Turbulent		

REFERENCES

- [1] American Institute of Aeronautics and Astronautics, 'AIAA' Report, 'Computational Study of Horizontal Axis Wind Turbines', the 12th International Conference on Machine Design and Production, Kuadasi, Turkey, 1999.
- [2] Annual Report IEA, International Energy Agency (IEA), 'Wind Energy', NREL/SP-440-7810, 1994.
- [3] M.S. Brower, M.W. Tennis, E.W. Denzler and M. Kaplan, 'Powering the Midwest: Renewable Electricity for the Economy and the Environment', Cambridge, MA: Union of Concerned Scientists, 188, 1993.
- [4] A.J. Cavallo, S.M. Hock and D.R. Smith, 'Wind Energy : Technology and Economics', Chapter 3 in Renewable Energy: Sources for Fuels and Electricity, Edited by Washington, DC: Island Press, 121-156, 1993.

- [5] J.L. Tangler, B. Smith and D. Jager, '*SERI Advanced Wind Turbine Blades*', NREL/TP-257-4492, Golden, CO, 1992.
- [6] R. Eppler, '*Airfoil Design & Data*', New York, NY, Springer-Verlag, 562, 1990.
- [7] M.S. Selig, J.F. Donovan and D.B. Fraser, '*Airfoils at Low Speeds*', Soartech 8, Virginia Beach, VA: H. A. Stokely, 398, 1989.
- [8] A.C. Hansen and C.P. Butterfield, '*Aerodynamics of Horizontal-Axis Wind Turbines*', Annual Review of Fluid Mechanics, Vol. 25, pp. 115 - 149, 1993.
- [9] J.G. Leishman and T.S. Beddoes, '*A Semi-Empirical Model for Dynamic Stall*', Journal of the American Helicopter Society, Vol. 34, pp. 3 - 17, 1989.
- [10] F.R. Menter, '*Two-Equation Eddy-Viscosity Turbulence Models for Engineering Applications*', American Institute of Aeronautics and Astronautics Journal, 'AIAA J.', Vol. 32, N°8, pp. 1598 - 1605, 1994.